Available online at www.sciencedirect.com

ScienceDirect

Procedia Engineering 88 (2014) 222 – 229

Procedia Engineering

www.elsevier.com/locate/procedia

International Symposium on Dynamic Response and Failure of Composite Materials, DRaF2014

STACKING SEQUENCE EFFECTS ON DAMAGE ONSET IN COMPOSITE LAMINATE SUBJECTED TO LOW VELOCITY IMPACT.

A. Riccio, G. Di Felice, S. Saputo, F. Scaramuzzino

Dpt. of Aerospace and Mechanical Engineering, Second University of Naples, via Roma, 29, Aversa (CE), Italy

Abstract

In this paper, the effects of the stacking sequence on the mechanical behavior of composite laminates subjected to low velocity impacts is investigated, taking into account inter-laminar and intra-laminar damage onset and evolution. The response of the composite laminate configurations characterized by different stacking sequences subjected to low velocity impacts with different impact energies have been studied to estimate the influence on the load-time, displacement-time and energy-time histories. A Finite element (FE) model has been used to numerically simulate the behavior of the composite plates. ABAQUS/EXPLICT FE environment has been considered for the implementation and the analyses and cohesive elements have been adopted to model the inter-laminar damage formation and evolution in the analyzed composite plate.

Peer-review under responsibility of the Organizing Committee of DRaF2014

Keywords: Low velocity impact, composite material, Abaqus FEM, cohesive elements

1. Introduction

The increasing need of materials with high specific mechanical properties and low specific weight has driven the development of composite materials. The search for structural elements able to absorb impact energy has been carried out by several industries as aeronautical, railway, naval and automotive. The general manufacturing process of composite material components, restricts the stacking sequence combination to laminates with 90, ±45, 0 oriented plies. Clustering of plies becomes unavoidable to comply with certain directional stiffness requirements. Although a laminate might have good stiffness properties, it may show a poor response to impact loads in particular when plies with the same orientations are packed together. The impact damage response is evaluated for final designs that meet the static load [23-28] and it is not accounted in the early design phase. However, there might be a significant margin to improve the impact response of a laminate designed to withstand in-plane loads, just by varying its

Peer-review under responsibility of the Organizing Committee of DRaF2014
doi:10.1016/j.proeng.2014.11.148

stacking sequence. The influence of stacking sequence of laminated composite plates, on the low velocity impact behavior, has been studied by several authors [1-11]. In low velocity impact phenomena the delaminated area is highly dependent on the out-of-plane displacement. This means that the bending stiffness plays an important role on the way the damage develops on an impacted laminate. In this paper the effect of the stacking sequence on the inter-laminar and intra-laminar damage onset and evolution has been evaluated. A detailed FE model of the panel has been developed in ABAQUS/EXPLICIT FEM code. The Hashin [30-32] failure criteria implemented in the adopted FE code have been used to predict the intra-laminar damage, while the inter-laminar-damage between adjacent plies has been simulated by means of cohesive elements [29-33].Two different impact energy levels and two stacking sequences have been considered, in order to better understand the influence of stacking sequence on the stiffness, and on the inter-laminar and intra-laminar damages formation and evolution.

2. Damage modelling

In impacted composite plates the prediction of intra-laminar damage has been performed by considering energy criteria based on Continuum Damage Mechanisms (CDMs)[23-28]. The intra-laminar damage models implemented in the FE code used in this work are based on several assumptions: the damage process is calibrated over the finite element dimension, the initiation and evolution criteria (based on an energy criteria) are defined for each failure mode and a damage variable is introduced which quantifies the damage occurring in terms of matrix and fiber traction and compression stiffness degradation .
Abaqus uses Hashin's failure criterion formulation [10-11] to evaluate the intra-laminar damage in composite laminates. The damage initiation criteria have the following general form shown in figure 1:

FAILURE CRITERIA	FAILURE MODES
$\left(\frac{\sigma_{11}}{X_t}\right)^2+\alpha\left(\frac{\tau_{12}}{S_l}\right)^2=1$	Fiber Tensile failure
$\left(\frac{\sigma_{11}}{X_c}\right)^2=1$	Fiber Compressive failure
$\left(\frac{\sigma_{22}}{Y_t}\right)^2+\left(\frac{\tau_{12}}{S_l}\right)^2=1$	Matrix Tensile failure
$\left(\frac{\sigma_{22}}{2S_t}\right)^2+\left[\left(\frac{Y_c}{2S_t}\right)^2-1\right]\left(\frac{\sigma_{22}}{Y_c}\right)+\left(\frac{\tau_{12}}{S_l}\right)^2=1$	Matrix Compressive failure

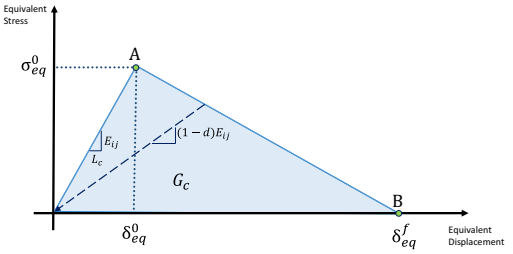

Fig. 1 Constitutive relation adopted for each failure mode

The coefficient α allows to take into account the shear stress contribution in the fiber tensile failure mode (indeed α=0 was set in this work). In Figure 1, the progressive damage bilinear model implemented in Abaqus FE code for each failure mode is also shown. According to the Hashin's failure criteria, the point A in Figure 1 represents the initiation of stiffness material degradation, before this point the material is undamaged. The damage propagation for each element start from the point A up to point B where the element is totally degraded. The parameter d_I represents the reduction of the stiffness for the failure mode I. It is possible to evaluate this parameter by the following relation:

$$d_I = \frac{\delta^f_{I,eq}\left(\delta_{I,eq}-\delta^0_{I,eq}\right)}{\delta_{I,eq}\left(\delta^f_{I,eq}-\delta^0_{I,eq}\right)} \quad ; \quad \left(\delta^0_{I,eq} \le \delta_{I,eq} \le \delta^f_{I,eq}\right) \quad I \in (f_c, f_t, m_c, m_t) \tag{1}$$

Where :

- $\delta^0_{I,eq}$ is the equivalent displacement at which the initiation criterion is satisfied.
- $\delta_{I,eq}$ is the equivalent displacement at which the material is complete damaged ($d_I = 1$).
- $\delta^f_{I,eq}$ is obtained by eq.2, by assuming that the fracture energy G_c is specified and the softening is linear:

$$\delta^f_{I,eq} = \frac{2G_{Ic}}{\sigma^0_{I,eq}} \tag{2}$$

$\sigma^0_{I,eq}$ is the equivalent stress at which the initiation criterion is verified. More details are available in the Abaqus FE code Manuals [33].

3. Interlaminar Failure

To study the formation and evolution of the inter-laminar damage in composite material, cohesive interface elements have been introduced between each ply. The stress failure criterion used to estimate the delamination onset is given by the Quadratic nominal stress Criterion law [10]:

$$\left(\frac{\sigma_n}{N_{max}}\right)^2 + \left(\frac{\sigma_t}{T_{max}}\right)^2 + \left(\frac{\sigma_s}{S_{max}}\right)^2 = 1 \qquad (3)$$

N_{max} is the Nominal stress in the pure normal mode, T_{max} is the Nominal stress in the first shear direction and S_{max} is the Nominal stress in the second shear direction. Where σ_i (i=n,s, t) denotes the traction stress vector in the normal and shear directions. The traction stress σ_i can be calculated as in [33] for modes I, II and III and the opening and/or sliding displacements δ_i:

$$\sigma_i = K_i \delta_i \qquad i = n, s, t \qquad (4)$$

When the relation (3) is satisfied the material stiffness is gradually degraded. The damage variables for each failure mode is given by the following relation:

$$d_I = \frac{\delta^f_{I,eq}\left(\delta_{I,eq} - \delta^0_{I,eq}\right)}{\delta_{I,eq}\left(\delta^f_{I,eq} - \delta^0_{I,eq}\right)} \quad ; \qquad \left(\delta^0_{I,eq} \le \delta_{I,eq} \le \delta^f_{I,eq}\right) \quad I \in (f_c, f_t, m_c, m_t) \qquad (5)$$

where $\delta^0_{I,eq}$ is the equivalent displacement at which the initiation criterion is satisfied, and $\delta_{I,eq}$ is the equivalent displacement at which the material is fully damaged ($d_I = 1$). The $\delta_{I,eq}$ parameter corresponds to the total mixed-mode displacement (normal, sliding, tearing) given by:

$$\delta_{I,eq} = \sqrt{\delta_n^{\,2} + \delta_s^{\,2} + \delta_t^{\,2}} \qquad (6)$$

A typical linear traction-separation model used for fracture Modes I, II and III is shown in Fig. 2. Initially, the linear elastic response is represented using the stiffness K_i ($i = n, s, t$). Once the normal or shear tractions reach the corresponding inter-laminar normal and shear strengths, delamination is initiated and then the stiffness is linearly degraded according to the damage evolution variable given by Eq.(5).

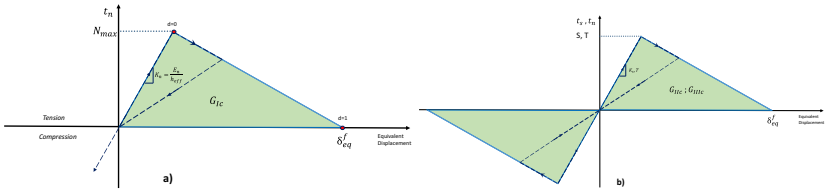

Fig. 2 Traction-separation law for cohesive material. A) for mode I and b) for mode II/III

The stiffness K_n, characterizing the initial damage phase, can be determined from the material stiffness E_n by introducing a penalty factor [17] or rather assuming that the behaviour of the cohesive element is the same of the matrix itself. In this paper the cohesive stiffness in the normal direction is imposed equal to elastic modulus of

matrix along the transversal direction divided by cohesive numerical thickness $K_{nn} = E_2/h_{eff}$, while the cohesive stiffness in the first and in the second shear directions is imposed equal to the matrix shear modulus divided by cohesive thickness $K_{ss} = K_{tt} = G/h_{eff}$.

4. **FEM Model**

As alredy mentioned, the finite element model has been built in the FE code Abaqus/Explicit [19-20]. The panel has been modelled by using the continuum shell element formulation available in the Abaqus database. Each element has eight nodes with three degrees of freedom at each node and one integration point. To better predict the onset and growth of the intra-laminar damage, each ply has been modelled with two continuum shell elements along the thickness. Localized stiffness reduction due to the presence of failed elements has been guaranteed by element deletion during the analysis. Interface between plies has been modelled thanks to cohesive element included in the Abaqus element database. Finite thickness cohesive elements have been placed at the interface between each ply. The plate was clamped between two holed rigid plates, modelled with 3D brick elements. The impactor has been modelled as a hemispherical 3-D rigid body. The diameter was set to 15 mm, the mass of the impactor have been set to 1Kg and 1.5 Kg to obtain the same initial velocity, in the vertical direction, for the two different energy value (see Figure 3). Contact pairs, using a penalty formulation, included in Abaqus/Explicit have been used to simulate the contact between the impactor and the laminate. Friction has been introduced between all the contacting surfaces. The friction coefficient between surfaces depends on the materials in contact, interface angle orientation and surface roughness, as demonstrated by several authors [15-17]. In this work an average friction coefficient of 0.5 has been used for all the interfaces between components made of the same material. On the other hand, a friction coefficient of 0.3 has been used for different materials in contact. Figure 4 shows the two different stacking sequence configurations used in this paper. For all the numerical models the material properties reported in Table 1 have been considered.

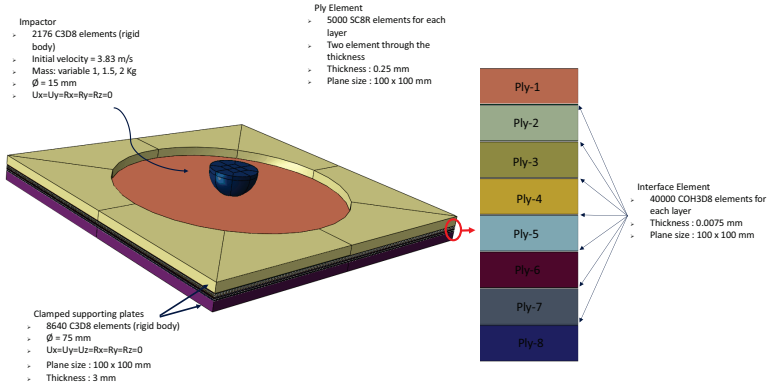

Fig. 3 Numerical Model

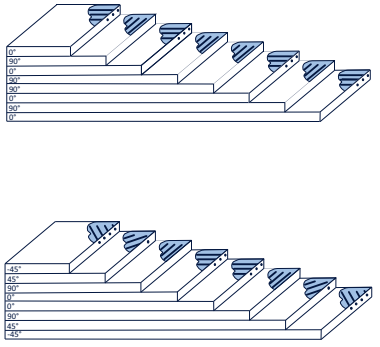

Fig. 4 Stacking sequence

As mentioned, the inter-laminar damage has been simulated by means of conveniently positioned cohesive element layers between each pair of plies. The "tie-constraints" method allowed to link the non-coincident meshes of solid and cohesive elements, using different sizes and element shapes for continuum shell elements and cohesive elements. This approach allows to refine the cohesive element layers in order to obtain more accurate predictions of the delamination shape without increasing the number of continuum shell elements with a reduction of the computational cost.

Intralaminar model Properties	
Density(ton/mm^3)	1.6e-9

Orthotropic property	E_1^0= 153 GPa; E_2^0=E_1^0=10.3 Gpa G_{12}^0=G_{13}^0= 6 GPa ; G_{23}^0= 3.7GPa ν_{12}=ν_{13}=0.3 ; ν_{23}=0.4
Ultimate stress	X^T=2537 ; Y^T= 82 ; X^C=1580 ; Y^C=263 S_{12}= 90 ; S_{23}=40
In-Plane fracture toughness (Kj/m^2)	G_{1C}^T=91.6 G_{1C}^C=79.9 ; G_{2C}^T=0.22 G_{2C}^C=1.1 G_s=0.7

Interlaminar model Properties

Density (ton/mm^3)		1.6e-9	
	Mode I	Mode II	Mode III
Normalised Elastic modulus (GPa/mm)	1373.3	493.3	493.3
Inter-laminar strength (MPa)	62.3	92.3	92.3
Inter-laminar fracture toughness (Kj/m^2)	0.28	0.79	0.79

Table 1 Material properties

5. **Results and conclusion**

In this section the simulations performed on the analysed two different stacking sequences for the considered two impact energies are presented and discussed. The mechanical behaviour of the numerical models is represented by the graph of the absorbed energy versus impact energy level. In Figure 5 and Table 2 the percentage of absorbed energy for the different configurations and impact energies is presented. In Figure 5 the graph is split in three regions representative of the composite plate impact behaviour: region 1 - the composite plate have a quasi-elastic behaviour, because the fraction of absorbed energy is very low (under 20%) as failure mechanisms are, in general not activated; region 2 - the composite plate shows some failure mechanisms, which are matrix crack and delaminations, so, the fraction of absorbed energy is intermediate (between 20% and 50%); region 3 - the composite plate shows many failure mechanisms, so the fraction of absorbed energy is very high, more than 50%.

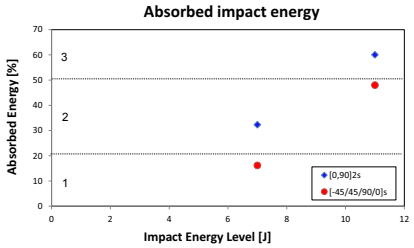

Fig. 5 Absorbed Energy

Impact Energy level [J]	Absorbed Energy	
	[0/90]2s	[-45/45/90/0]s
7J	32.28	19
11J	60	40.27

Table 2 Absorbed Energy

In Figures 6 and 7 and in Figures 8 and 9, The impact Force-Time and the Force-Displacement curves for the analysed stacking sequences and impact energies are reported. Intense oscillations occurring near the peak force value indicate initiation of damage. For plates that includes 45 and -45 oriented plies the peak impact force was higher than the configuration with 0/90 oriented ply, for both the impact energy value. This result highlights the influence of stacking sequence on the bending stiffness of the plate. Indeed the configuration with [0/90]2s plies is less stiff than the other configuration. In Figure 10 and 11 the trends of internal energy are reported. From these figures it can be appreciated that, for both impact energies, the configuration [0/90]2s absorbs an amount of energy greater than the other configuration.

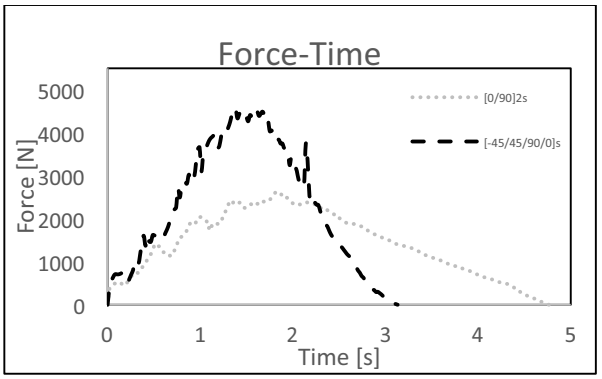

Fig.6 Force-time, 7 J impact energy

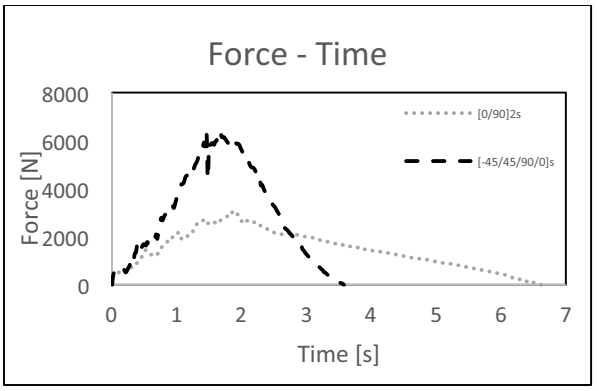

Fig. 7 Force-time, 11 J impact energy

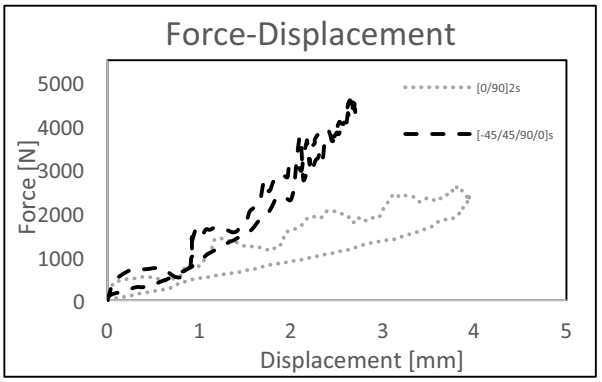

Fig. 8 Force-Displacement, 7 J impact energy

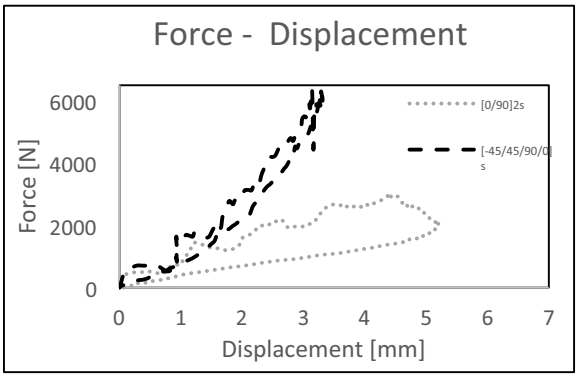

Fig 9 Force-Displacement, 11 J impact energy

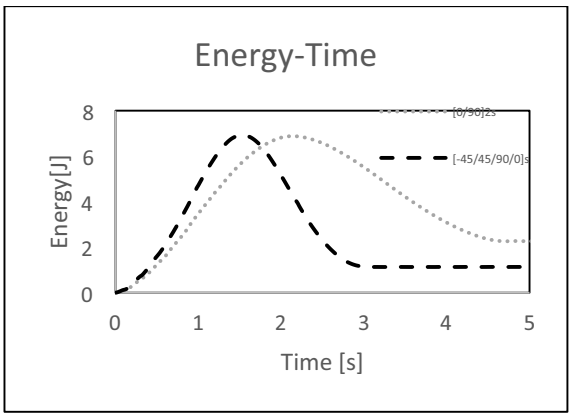

Fig. 10 Energy-Time, 7 J impact energy

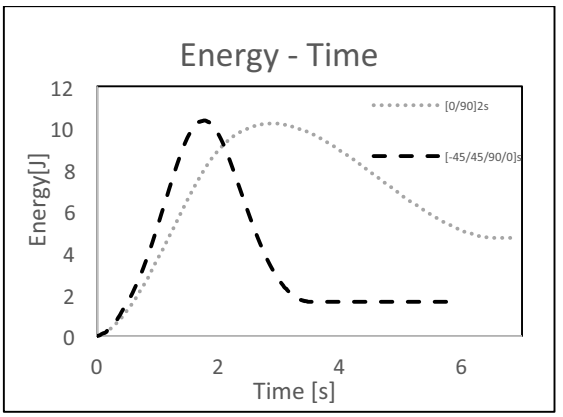

Fig. 11 Energy-Time, 11 J impact energy

The final absorbed energy as inter-laminar and intra-laminar damage with different impact energies and for different stacking sequences are better represented by figures 12-15. In these figures the damaged interface elements and the

damaged ply elements are shown for the analysed stacking sequence configurations and impact energies. The formation of delaminations generally relates to matrix cracking. For the analysed models, it can be appreciated how the delamination is influenced by the breaking of the underlying ply matrix. The matrix damage of the single ply is obviously influenced by the considered stacking sequence.

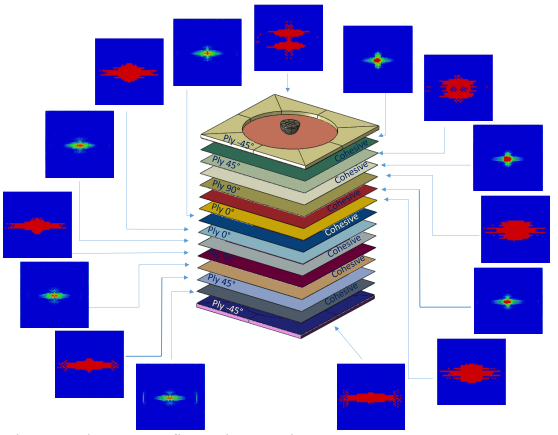

Fig. 12 [0/90]2s configuration 7 J impact energy

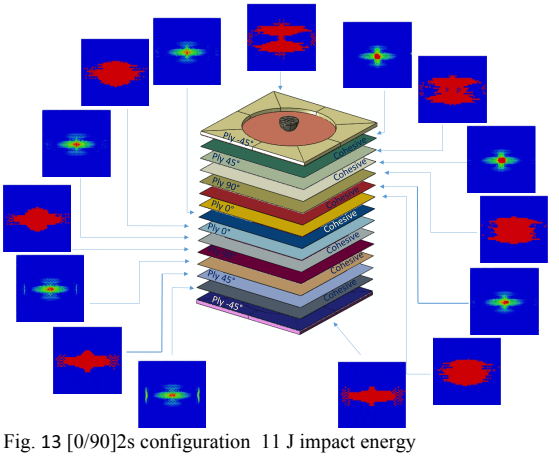

Fig. 13 [0/90]2s configuration 11 J impact energy

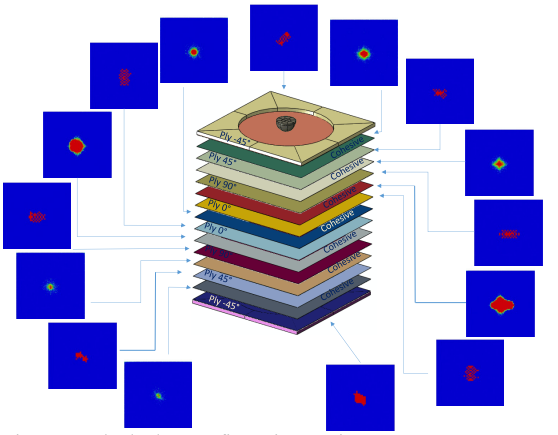

Fig. 14 [-45/45/90/0]s configuration 7 J impact energy

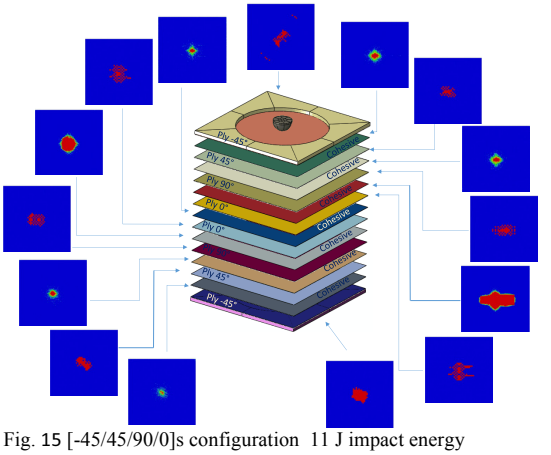

Fig. 15 [-45/45/90/0]s configuration 11 J impact energy

Finally, in Figures 16 and 17 the overlapped images of the inter-laminar damages throughout the whole lay-up, for the impact energies and for the considered stacking sequence, are reported. As expected, the delaminations for a given stacking sequence increase with the increase of the impact energy, keeping the same shape.

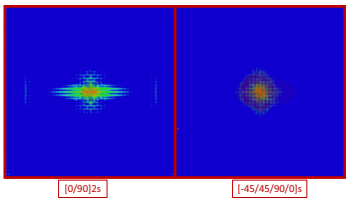

Fig. 16 Delamination 7 J

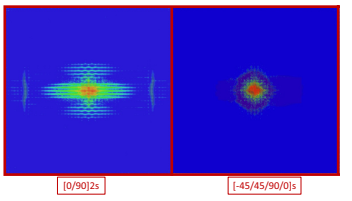

Fig. 17 Delamination 11 J

6. References

[1] Abrate S. Impact on composite structures. Cambridge (UK): Cambridge University Press; 1998.
[2] Pietropaoli E and RiccioA. On the robustness of finite element procedures based on Virtual Crack Closure Technique and fail release approach for delamination growth phenomena. Definition and assessment of a novel methodology. Comp. Sci. Tech 2010;70(8):1288-1300.
[3] Pietropaoli E and Riccio A. Formulation and assessment of an enhanced finite element procedure for the analysis of delamination growth phenomena in composite structures. Composite Science and Technology 2011;71(6):836-846.
[4] Pietropaoli E and Riccio A. A Global/Local Finite Element Approach for Predicting Interlaminar and Intralaminar Damage Evolution in Composite Stiffened Panels Under Compressive Load. Applied Composite Materials 2011;18(2):113-125.
[5] Armentani E, Caputo F, Esposito and Godono G. Evaluation of energy release rate for delamination defects at the skin/stringer interface of a stiffened composite panel. Eng. Fract. Mech. 2004;71(4-6):885-895.
[6] Caputo F, Esposito R, Perugini P and Santoro D. Numerical-experimental investigation on post-buckled stiffened composite panels. Composite Structures 2002; 55(3):347-357.
[7] Riccio A, Raimondo A and Scaramuzzino F. A study on skin delaminations growth in stiffened composite panels by a novel numerical approach. Appl. Comp. Mat. 2013;20(4):465-488.
[8] Riccio A, Raimondo A, Borrelli R, Mercurio U, Tescione D and Scaramuzzino F. Numerical Simulations of Inter-laminar damage evolution in a composite wing box. Applied Composite Materials 2013; DOI: 10.1007/s10443-013-9347-2
[9] Pietropaoli E and Riccio A. Finite element analysis of the stability (buckling and post-buckling) of composite laminated structures: well established procedures and challenges. Applied Composite Materials 2012;19:79-96.
[10] Riccio A, Scaramuzzino F and Perugini P. Influence of Contact Phenomena on Embedded Delamination Growth in Composites. AIAA Journal 2003;41(5):933-940.
[11] Riccio A, Raimondo A and Scaramuzzino F. Skin stringer debonding evolution in stiffened composites under compressive load:A novel numerical approach; KEM 2014;77-578:605-608.
[12] Batra RC, Hassan NM. Blast resistance of unidirectional fiber reinforced composites. Composites B 2008;39:513–36.
[13] Batra RC, Hassan NM. Response of fiber reinforced composites to underwater explosive loads. Composites B 2007;38:448–58.
[14] Kachanov L. On the creep rupture time. Izv Akad Nauk SSSR 1958;8:26–31.
[15] Rabotnov Y. On the equations of state for creep. Progress in applied mechanics. Prager Anniversary vol. New York: Macmillan; 1963.
[16] Talreja RA. Continuum mechanics characterization of damage in composite materials. Proc Royal Soc London 1985;399:195–216.
[17] Ladeveze P. A damage method for composite structures. Comp.. Struct. 1992;4:79–87.
[18] Barberis U, Hassim A, Ravera C and Vanderborck G. Impact-induced damage analysis tool for composites. Advances in composite materials and structures VII. Boston: WIT Press; 2000.
[19] Riccio A, Di Felice G, LaManna G, Antonucci V, Caputo F, Lopresto V and Zarrelli M. A global-local numerical model for the prediction of Impact Induced Damage in Composite Laminates. Applied Composite Materials 2013; DOI: 10.1007/s10443-013-9343-6.
[20] Riccio A, Di Felice G, Saputo S and Scaramuzzino F. A Numerical Study on Low velocity impact induced damage in stiffened composite panels. Journal of Computational Simulation and Modeling 2013; 3(1):044-047.
[21] Caputo F, Di Gennaro F, Lamanna G, Lefons A and Riccio A. Numerical procedures for damage mechanisms analysis in CFRP composites. Key Eng. Mat. 2013; 569-570:111-118
[22] Riccio A, Russo T and Scaramuzzino F. Impact Damage Management of Composite Laminated Structures by a Probabilistic Approach. The Open Materials Science Journal 2013;7:8-22.
[23] Riccio A, RaimondoA, Fragale S, Camerlingo F, Gambino B, Toscano C and Tescione D. Delaminations buckling and growth phenomena in stiffened composite panels under compression. Part I: an Experimental Study. Journal of Composite Materials 2013; DOI:10.1177/0021998313502741
[24] Riccio A, Raimondo A, Di Caprio F and Scaramuzzino F. Delaminations buckling and growth phenomena in stiffened composite panels under compression. Part II: a Numerical Study. Journal of Composite Materials 2013; DOI:10.1177/0021998313502742.
[25] Toscano C, Riccio A, Camerlingo F and Meola C. On the use of Lockin Thermography to Monitor Delamination Growth in Composite Panels under Compression. Science and Engineering of Composite Materials 2013; DOI: 10.1515/secm-2013-0156.
[26] De Angelis G, Meo M, Almond DP, Pickering SG and Angioni SL. A comparison between optimized active thermography and digital shearography for detection of damage in aerospace composite structures. RILEM Bookseries 2012; 6:641-647. ISSN: 22110844.
[27] De Angelis G, Meo M, Almond DP, Pickering SG and Angioni SL. A new technique to detect defect size and depth in composite structures using digital shearography and unconstrained optimization. NDT and E International 2012;45(1):91-96.
[28] Polimeno U, Meo M, Almond DP and Angioni SL. Detecting low velocity impact damage in composite plate using nonlinear acoustic/ultrasound methods. App. Comp. Mat. 2010;17(5):481-488.
[29] Camanho PP, Davila CG. Mixed-mode decohesion finite elements for the simulation of delamination in composite materials. 2002; NASA/TM-2002–211737, pp. 1–37
[30] Hashin Z and Rotem A. A Fatigue Criterion for Fiber -Reinforced Materials. J. Comp. Mat. 1973;7:448–464.
[31] Hashin Z. Failure criteria for unidirectional fiber composites. J. Appl. Mech. 1980;47:329-334.
[32] ABAQUS Analysis User's Manual 6.11, 2011
[33] Bazant ZP and Oh BH. Crack band theory for fracture of concrete. Mat Struc. 1983;16:155–77.